The Astrophysical Journal, 652:1339–1347, 2006 December 1

MAGNETICALLY DOMINATED STRANDS OF COLD HYDROGEN IN THE RIEGEL-CRUTCHER CLOUD

N. M. McClure-Griffiths,[1] J. M. Dickey,[2] B. M. Gaensler,[3,4] A. J. Green,[5] and Marijke Haverkorn[6,7]

Received 2006 June 13; accepted 2006 August 26

ABSTRACT

We present new high-resolution (100″) neutral hydrogen (H I) self-absorption images of the Riegel-Crutcher cloud obtained with the Australia Telescope Compact Array and the Parkes Radio Telescope. The Riegel-Crutcher cloud lies in the direction of the Galactic center at a distance of 125 ± 25 pc. Our observations resolve the very large, nearby sheet of cold hydrogen into a spectacular network of dozens of hairlike filaments. Individual filaments are remarkably elongated, being up to 17 pc long with widths of less than ∼0.1 pc. The strands are reasonably cold, with spin temperatures of ∼40 K and in many places appearing to have optical depths larger than 1. Comparing the H I images with observations of stellar polarization, we show that the filaments are very well aligned with the ambient magnetic field. We argue that the structure of the cloud has been determined by its magnetic field. In order for the cloud to be magnetically dominated the magnetic field strength must be >30 μG.

Subject headings: ISM: atoms — ISM: clouds — ISM: magnetic fields — ISM: structure — radio lines: ISM

1. INTRODUCTION

Recent high-resolution surveys of neutral hydrogen (H I) in the Galactic plane show that the structure of the warm atomic medium varies significantly on arcminute scales. The detailed structure of cold H I, however, is much more elusive. Most of our knowledge of cold H I comes from observations of H I absorption toward continuum sources (e.g., Heiles & Troland 2003, 2005). Although these measurements are effective for determining gas temperature, they have limited applicability to structural studies because they only trace gas along single lines of sight toward an irregularly distributed array of background sources. Another probe of cold H I is H I self-absorption (HISA) toward bright background H I emission. This is not, strictly speaking, self-absorption, but absorption of background H I emission by cold foreground H I. Surveys such as the Canadian Galactic Plane Survey (CGPS; Taylor et al. 2003) and the Southern Galactic Plane Survey (SGPS; McClure-Griffiths et al. 2005) have revived studies of HISA, showing that it is a good probe of the structure of cold H I on small scales (e.g., Gibson et al. 2000; Kavars et al. 2005). Although these studies are able to image HISA over large areas, and have better estimates of the background emission than lower resolution surveys, it remains difficult to unravel the structure of the cold foreground H I from variations in the background emission.

One of the most famous examples of a large-scale HISA feature is the Riegel-Crutcher (hereafter R-C; Riegel & Crutcher 1972) cloud in the direction of the Galactic center. The R-C cloud was first discovered by Heeschen (1955) in his survey of H I at the Galactic center, and he suggested that the cloud was very extended. Subsequent observations by Riegel & Jennings (1969) showed that the cold cloud extends over ∼40° of Galactic longitude and ∼10° of latitude. It has even been suggested that the cloud is part of a much larger structure, Lindblad's Feature A, spanning the full 360° of Galactic longitude (Lindblad et al. 1973). Estimates of the temperature of the cloud show that despite its striking appearance it is not exceptionally cold, with most estimates of spin temperature ranging between 35 and 45 K (Montgomery et al. 1995; Riegel & Crutcher 1972; Riegel & Jennings 1969; Heeschen 1955). By measuring Ca II lines in the spectra of OB stars Crutcher & Riegel (1974) determined that the cloud is between 150 and 180 pc distant. Further Na I observations by Crutcher & Lien (1984) helped constrain the distance to 125 ± 25 pc, with an estimated thickness of 1–5 pc.

The R-C cloud provides us with one of the best opportunities for imaging the cold neutral medium (CNM) over a large area. The H I background toward the center of the Galaxy is among the brightest anywhere in the Galaxy; this direction provides an ideal bright, high column density background against which to image the CNM. Here we present new high-resolution (∼100″) H I images of the R-C cloud, which allow us to study the structure of the CNM on scales of 0.06 to 22 pc. In this paper we explore the relationship of the R-C cloud to the ambient magnetic field and discuss its implications for the structure of the CNM throughout the Milky Way.

This paper is structured as follows. In § 2 we discuss the data taking and reduction strategy used. In § 3 we present images of the R-C cloud, and in § 3.1 we derive optical depth and column density maps. We present evidence of an associated magnetic field in § 4. In § 5.1 we discuss the strength of the magnetic field and its effect on the structure of the cloud. In §§ 5.2 and 5.3 we comment on the structure of the R-C cloud, its similarity to molecular clouds and the implications for models for the structure of the CNM.

2. OBSERVATIONS AND DATA ANALYSIS

The data presented here were obtained as part of an extension to the SGPS (McClure-Griffiths et al. 2005). Between late 2002 and early 2004 the SGPS was extended to cover 100 deg^2 around the Galactic center. The SGPS Galactic Center (GC) survey, like the main SGPS, is a survey of the 21 cm continuum and H I

[1] Australia Telescope National Facility, CSIRO, P.O. Box 76, Epping NSW 1710, Australia; naomi.mcclure-griffiths@csiro.au.
[2] School of Mathematics and Physics, University of Tasmania, Private Bag 21, Hobart TAS 7001, Australia; john.dickey@utas.edu.au.
[3] Alfred P. Sloan Fellow; Harvard-Smithsonian Center for Astrophysics, 60 Garden Street, Cambridge, MA 02138.
[4] Current address: School of Physics, The University of Sydney A29, NSW 2006, Australia; bgaensler@physics.usyd.edu.au.
[5] School of Physics, The University of Sydney A29, NSW 2006, Australia; agreen@physics.usyd.edu.au.
[6] Astronomy Department, University of California, 601 Campbell Hall, Berkeley, CA 84720; marijke@astro.berkeley.edu.
[7] Jansky Fellow, National Radio Astronomy Observatory.

TABLE 1
SGPS Galactic Center ATCA Observations

Dates	Array Configuration
2002 Dec 21–31	EW367
2003 Mar 24–31	EW352
2003 May 11–13	EW352
2003 Jun 27–29	750C
2003 Aug 11–15	EW367
2003 Sep 11–19	750C
2004 Feb 19–Mar 1	750A
2004 Jun 2– 14	750D
2004 Nov 13	750C[a]

[a] Make-up session.

spectral line emission in large regions of the Galactic plane. The GC survey covers $-5^\circ \leq l \leq +5^\circ$ and $-5^\circ \leq b \leq +5^\circ$. The main goal of the SGPS GC survey is to study the structure and dynamics of H I in the inner $\sim$1 kpc of the Galaxy, a topic that we will defer to a future paper.

The GC survey combines data from the Australia Telescope Compact Array (ATCA) and the Parkes Radio Telescope for full sensitivity to angular scales from 10° down to the $100''$ resolution of the data. The Parkes data were observed and imaged as part of the main SGPS survey and are fully described in McClure-Griffiths et al. (2005). The ATCA data were taken in a slightly different manner than the data for the rest of the SGPS. For completeness we describe the full ATCA GC survey parameters here.

The ATCA is an interferometer of six 22 m dishes situated near Narrabri, New South Wales, Australia. ATCA data were obtained during eight observing sessions between 2002 December and 2004 June. An additional day of make-up observations was scheduled in 2004 November to fill in gaps in the *u-v* coverage. The ATCA has linear feeds that receive two orthogonal linear polarizations, *X* and *Y*, and can observe at two intermediate frequencies (IFs) simultaneously. As in the SGPS, all data were recorded using a correlator configuration that records the autocorrelations, *XX* and *YY*, in 1024 channels across a 4 MHz bandwidth, as well as the full polarization products, *XX*, *YY*, *XY*, and *YX*, in 32 channels across a 128 MHz bandwidth. The first IF was centered at 1420 MHz to observe the H I line and the second was centered at 1384 MHz. Here we describe only the narrowband H I data and reserve discussion of the continuum data for a future paper.

Observations were made using six east-west array configurations with maximum baselines between 352 and 750 m. Most baselines, in multiples of 15 m, between 31 and 750 m were sampled by the combination of the configurations EW352, EW367, 750A, 750B, 750C, and 750D. The observing arrays and dates are given in Table 1. The 100 deg^2 field was covered by a total of 967 individual pointings; 948 pointings were newly observed and the remaining 19 pointings were taken from the SGPS Phase I. All pointings were distributed on a common hexagonal pattern with a separation of $19'$ between adjacent pointings. The observations were made in snapshot mode with 60 s integrations per pointing. Each pointing was observed approximately 30 times for a total integration time of $\sim$30 minutes per pointing.

The primary flux calibrator, PKS B1934−638, was observed once per day for bandpass and absolute flux calibration, assuming a flux at 1420 MHz of 14.86 Jy (Reynolds 1994). A secondary calibrator, PKS B1827−360, was observed approximately every 45 minutes for complex gain and delay calibration. Data editing and calibration were completed within the MIRIAD data reduction package using standard techniques (Sault & Killeen 2004).

The 967 pointings were linearly combined and imaged using a standard grid-and-FFT (fast Fourier transform) scheme. The mosaicing process uses the joint approach, where dirty images are linearly combined and jointly deconvolved (Sault et al. 1996). The joint imaging and deconvolution process improves the sensitivity to large angular scale structures, increasing the maximum scale sampled from $\sim 23'$ for a single pointing observation to $\sim 30'$ for the mosaicked image (McClure-Griffiths et al. 2005). The deconvolution uses a maximum entropy method, which is very effective at deconvolving large-scale emission. The maximum entropy algorithm in MIRIAD does not deconvolve the dirty beam from areas of "negative emission," such as continuum sources observed in absorption. The Galactic center region contains many very strongly absorbed continuum sources that would not be deconvolved in standard processing. To reduce the confusing sidelobe levels observed around these sources we modeled the sources and subtracted them from the *u-v* data prior to imaging. Although we were not able to completely remove the sources, the resultant sidelobes were significantly reduced and do not adversely affect the analysis of the H I cube presented here.

Finally, the deconvolved ATCA image cube was combined with the Parkes data cube to recover information on angular scales larger than $\sim 36'$. This combination was performed using the MIRIAD task IMMERGE, which Fourier transforms the deconvolved ATCA and Parkes images, reweights them such that the Parkes image is given more weight for large angular scales and the ATCA image more weight for small angular scales. The weighted, Fourier-transformed images are linearly combined and then inverse Fourier-transformed (Stanimirović 2002). The final data cube has a resolution of $100''$ and is sensitive to angular scales up to the 10° image size. The rms brightness temperature sensitivity in the combined cube is $\sim$2 K. The rms increases to $\sim$3 K in the $\sim$1 deg^2 immediately surrounding the Galactic center because the broad H I line emission contributes to the ATCA system temperature. Here we present only the part of the H I data cube pertaining to the Riegel-Crutcher cloud, the full SGPS GC data set will be published in a future paper.

3. RESULTS

An H I image at a local standard of rest (LSR) velocity of 4.95 km s^{-1} from the final, combined H I data cube is shown in the left panel of Figure 1. The Riegel-Crutcher (R-C) cloud is visible as the large black swath that extends from top left to the bottom right of the image. In order to estimate the properties of the cloud itself, and to better examine its structure, we need to separate it from the background H I emission. There are many ways of estimating the unabsorbed H I emission, $T_{\rm off}$, including using averages of spectra observed adjacent to the cloud or interpolating across the absorption with a linear, parabolic, or high-order polynomial fit. Each technique has its limitations; for very extended features like the R-C cloud, off cloud spectra are too distant from the on-cloud positions to accurately reflect the unabsorbed emission. High-order polynomial interpolations across the absorption profile can give good estimates for $T_{\rm off}$, but these are computationally expensive for many spectra. Depending on the line profile a simple linear fit can also give a reasonable approximation to the off-cloud emission, with minimal computational effort. For simplicity we have chosen to interpolate across the absorption with a linear fit. An example of an interpolated spectrum and the difference between the absorbed and unabsorbed

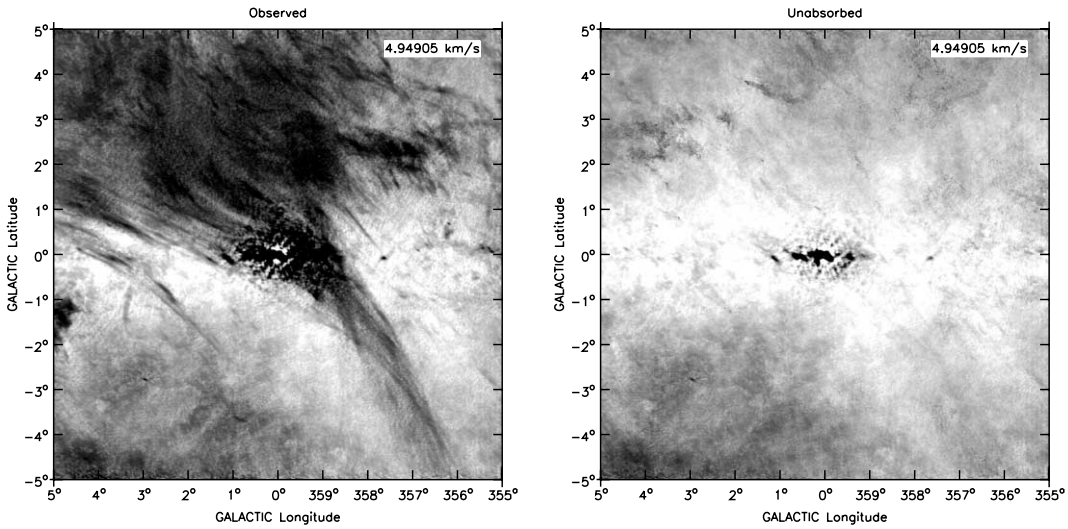

FIG. 1.—SGPS H I image at $v = 4.95$ km s^{-1} toward the Galactic center. The left panel shows the observed emission, and the right panel shows the interpolated estimation of the unabsorbed emission. The gray scale is the same in both images, ranging from 15 K (*black*) to 140 K (*white*). The angular resolution of these images is 100″.

spectra, $\Delta T \equiv T_{\rm on} - T_{\rm off}$, is shown in Figure 2. For each pixel in the GC cube with an absorption depth of more than 8 K we searched for the edges of the absorption feature, interpolated between those edges, and replaced the intermediate channels with the interpolated spectrum. The result is a cube of unabsorbed emission, $T_{\rm off}$. The right panel of Fig. 1 shows the unabsorbed emission for the same velocity channel as the left panel. Although the interpolation is not perfect, it has removed the bulk of the R-C cloud.

Velocity channel images of the difference, ΔT, between the observed and the unabsorbed cubes are shown in Fig. 3. Here we show only velocity channels between 3.3 and 7.4 km s^{-1}, which cover the majority of the R-C cloud at these longitudes. The images have a channel separation of 0.82 km s^{-1}. The bulk of the cloud is observed in the top left corner of the image, from there the cloud extends to higher longitudes and latitudes, not covered by the SGPS. In this region the cloud appears fairly smooth in structure. Extending from the bulk of the cloud toward the lower right of the image is a wispy elongated structure. Unlike the dense top of the cloud, the tail appears to be resolved into a network of narrow filaments, or strands, all roughly aligned. We emphasize that the edges of these filaments are real self-absorption features and are not simply places where the background emission drops away. The ensemble of filaments has a distinct curvature to it and resembles a rope of gas made up of individual strands. The individual strands appear to be mostly unresolved or in some cases marginally resolved. They have widths of between 2′ and 5′, which, at a distance of 125 pc, correspond to physical widths of 0.07–0.2 pc. Some filaments can be traced across the majority of the image; the longest continuous filament is 7.°7, or 16.9 pc. Many of the filaments have aspect ratios in the range (50–170):1.

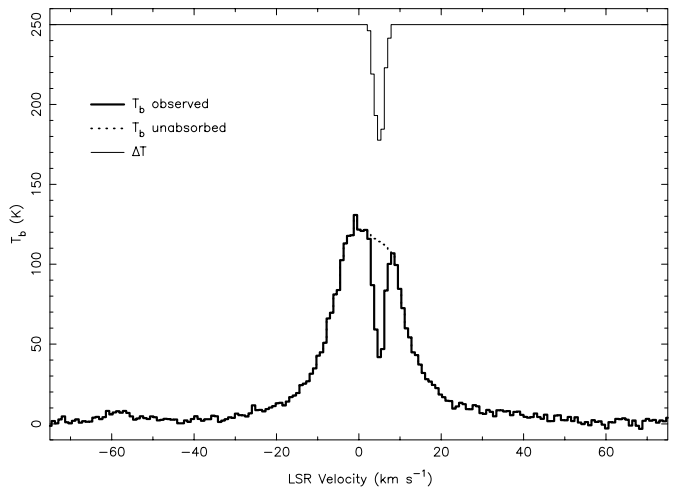

FIG. 2.—H I spectra toward $l = 0.°79$, $b = 1.°99$. The heavy solid line shows the observed spectrum, $T_{\rm on}$, the dotted line is the interpolated spectrum, $T_{\rm off}$, and the thin solid line is the difference $\Delta T = T_{\rm on} - T_{\rm off}$. The baseline of the difference spectrum has been offset by 250 K.

3.1. *Properties of the Cloud*

Deriving the temperature and density of an H I cloud is nontrivial. In theory these can be derived from solutions of the radiative transfer equation. In practice, however, the radiative transfer equation cannot be solved for the complicated H I profiles observed in the Galaxy. To derive the spin temperature, T_s, and optical depth, τ, of the R-C cloud we must make some simplifying assumptions. Here we use the four-component model outlined in Gibson et al. (2000) and Kavars et al. (2003). This model assumes that all of the continuum emission, T_c, originates behind the HISA cloud, but allows for both foreground and background H I with spin temperature and optical depths of $T_{s,\rm fg}$, $\tau_{\rm fg}$ and $T_{s,\rm bg}$, $\tau_{\rm bg}$ respectively. In this model, the radiative transfer equation can be solved for the difference between the observed brightness temperature on, $T_{\rm on}$, and off the cloud, $T_{\rm off}$. In the difference between on and off cloud the direct contribution to the brightness temperature from the foreground cloud is the same and cancels out. The on-off difference is given by

$$\Delta T \equiv T_{\rm on} - T_{\rm off} = \left[T_s - T_{s,\rm bg}\,\left(1 - e^{-\tau_{\rm bg}}\right) - T_c\right]\,\left(1 - e^{-\tau}\right). \quad (1)$$

All variables, with the exception of T_c, are functions of velocity, v. We make a further assumption that $\tau_{\rm fg}$ and $\tau_{\rm bg}$ are small. As in Gibson et al. (2000) we use the variable, p, to describe the fraction of the H I emission originating behind the self-absorption

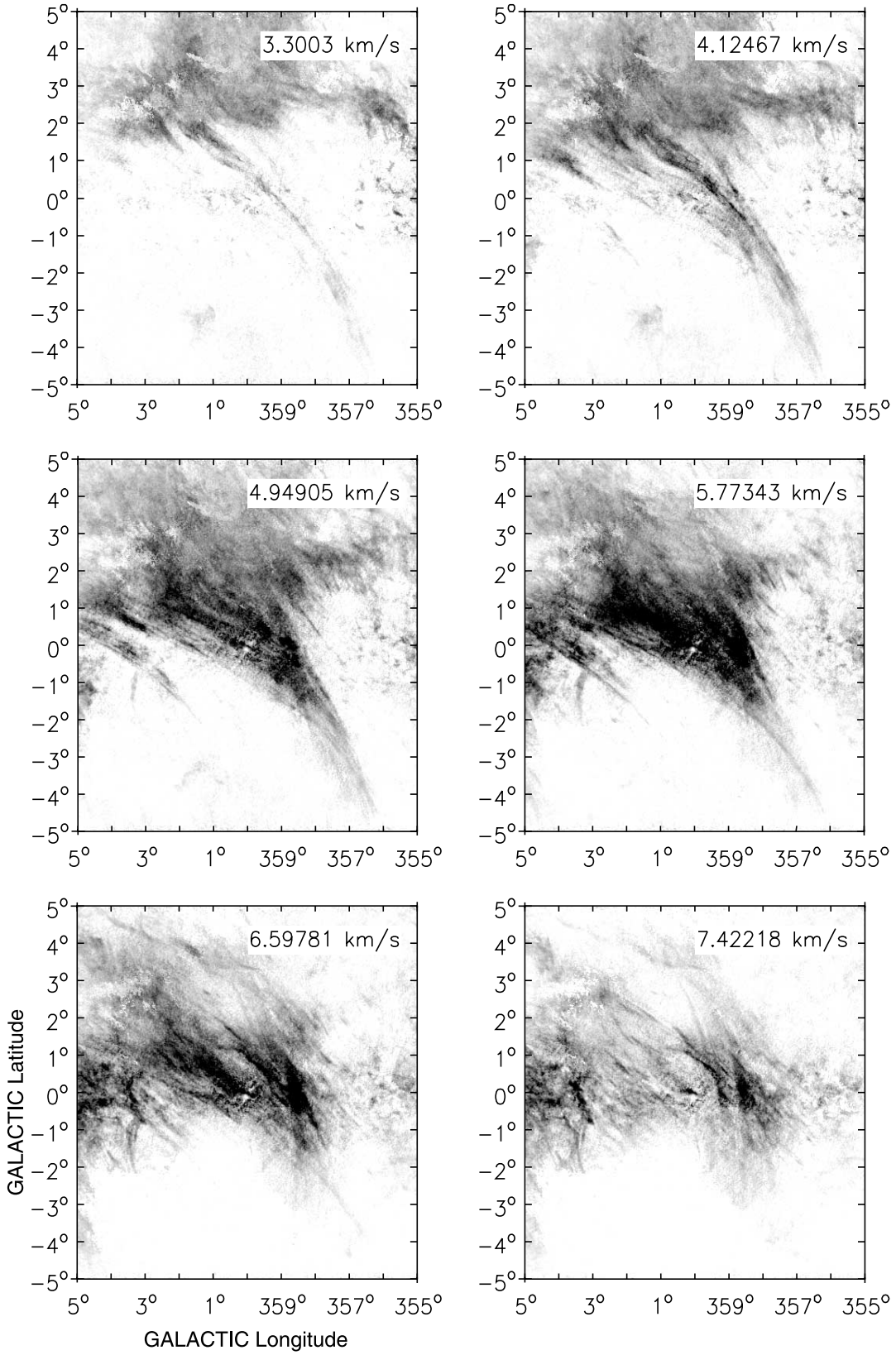

FIG. 3.—Velocity channel images of ΔT, the difference between the data and the interpolation, of the R-C cloud. Every channel from 3.3 to 7.4 km s^{-1} is shown. The LSR velocity of the channel is shown in the top right corner of the image. The gray scale is linear between 0 (*white*) and −120 K (*black*).

cloud. These assumptions allow us to solve equation (1) for the optical depth,

$$\tau = -\ln\left(1 - \frac{\Delta T}{T_s - T_c - pT_{\rm off}}\right), \qquad (2)$$

for a given value of p in the range $0 \leq p \leq 1$.

The continuum temperature, T_c, is measured from our Parkes continuum maps. Although these are at a much lower resolution than the ATCA data, the variation on small scales is only 10% of the mean continuum emission for a given latitude and not deemed important for the rough temperature analysis presented here. Included in equation (2) are the parameters $T_{\rm off}$ and p, which are not directly observed and must therefore be estimated. For $T_{\rm off}$ we use the interpolated cube described above. Although the technique of linear interpolation across the absorption feature can underestimate the absorption in the line wings, we find that the errors introduced are small when compared to ΔT. As our analysis does not rely heavily on accurate line widths, this does not significantly affect our results. To estimate p we assume that because the R-C cloud is at a distance of only 125 pc and lies just beyond the edge of the Local Bubble (Crutcher & Lien 1984), there is very little foreground H I emission and the majority of the H I emission will be behind the cloud. We therefore assume that p is constant across the cloud and that it is equal to one, which will give a lower limit for the optical depth. We discuss the implications on τ for nonunity values of p in § 3.1.2.

It is clear from equation (2) that the optical depth and spin temperature of the cloud are degenerate. Numerous authors have explored methods of constraining either T_s or τ, including some efforts applied specifically to the R-C. For example, Montgomery et al. (1995) estimated $T_s = 35$ K by assuming that all of the measured line width, Δv, for the narrowest absorption line can be attributed to random kinetic motions, so that $T_s = T_k = 21.6\ (\Delta v)^2$ K. This equation must be used with care, however, because it ignores all turbulent motions, which is not always an appropriate assumption. Spin temperature values estimated this way should be considered only as upper limits. This method also demands an accurate measurement of the line width, which as Levinson & Brown (1980) caution, can be difficult to attain for an H I self-absorption feature.

In some circumstances the line shape itself can be used to decouple T_s and τ. Assuming a Gaussian optical depth of width Δv, centered at v_c,

$$\tau(v) = \tau_0 \exp\left[-2 \ln 4 (v - v_c)^2 / \Delta v^2\right], \qquad (3)$$

the absorption profile defined by equation (1) will flatten in the core as $\tau > 1$. In this equation Δv is related to the line dispersion, σ, as $\Delta v = (8 \ln 2)^{1/2}\ \sigma$. To accurately trace the line shape requires high signal-to-noise absorption spectra (Levinson & Brown 1980), which are not generally available. Fortunately, the depth of the absorption toward the R-C cloud is so large that our observed absorption spectra have S/N ratios in excess of 80, which makes it possible to fit slightly flattened profiles. There are several regions in the R-C cloud where we observe slight saturation in the line profiles. An example is shown in Figure 4, where the line profile is slightly non-Gaussian near the core, showing signs of saturation. By assuming a value for p, we can fit the saturated profiles to uniquely measure τ and T_s. Fitting this profile to equation (1), where τ is given by equation (3), we find $\tau = 2.5$ and $T_s = 40$ K. The fit is shown in Figure 4 as the solid line. Fitted lines for constant values of $\tau = 3.5$ and $\tau = 1.5$ are also overlaid for comparison. Fitting all saturated profiles in the GC

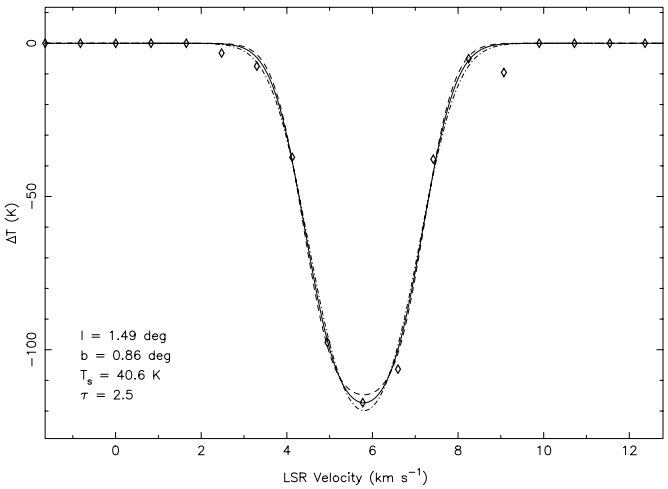

FIG. 4.—H I absorption spectrum at $(l, b) = (1.^\circ49,\ 0.^\circ86)$ toward the R-C cloud. The data points are shown with diamonds. The fit to the marginally saturated line shape given by $T_s = 40$ K and $\tau = 2.5$ is plotted with the solid line. For comparison, fits for $\tau = 3.5$, $T_s = 51$ K and $\tau = 1.5$, $T_s = 14$ K are shown with dashed and dashed-dotted lines. Fits for values of $\tau < 1$ result in nonphysical spin temperatures. The 1 σ errors on the individual points are approximately the size of the plotted diamond.

data set we find that the spin temperatures lie in the range 30–65 K. Because of the errors involved in this method for deriving spin temperatures these are only estimates of the temperature. Comparing the range of spin temperatures that we estimate with those estimated by Montgomery et al. (1995) and Crutcher & Lien (1984), we have chosen to adopt a spin temperature of $T_s = 40$ K for the R-C cloud. It is heartening to note that this is the same value that Heeschen (1955) found in his original work on this feature.

The fit to the line profile also gives us an estimate for the observed line width, $\sigma_{\rm obs}$. We assume that the measured line width is related to the thermal and turbulent line widths by $\sigma_{\rm obs} = (\sigma_{\rm turb}^2 + \sigma_{\rm th}^2)^{1/2}$. We find typical values across the cloud of $\sigma_{\rm obs} \sim 1.5$ km s^{-1}, which corresponds to a line FWHM of $\Delta v = (8 \ln 2)^{1/2} \sigma_{\rm obs} \sim 3.5$ km s^{-1}. For 40 K gas the thermal line width is $\sigma_{\rm th} \sim 0.6$ km s^{-1}, which allows us to approximate the turbulent line width as $\sigma_{\rm turb} \sim 1.4$ km s^{-1}.

3.1.1. *Density and Pressure*

The column density of the H I line is related to the spin temperature and optical depth by

$$N_{\rm H\,I} = 1.83 \times 10^{18}\ T_s \int \tau(v)\, dv\ {\rm cm}^{-2}, \qquad (4)$$

which is valid for small τ. Using a constant value for T_s across the cloud we can solve equation (2) for the optical depth as a function of position and velocity, which may be integrated to produce a column density image for the R-C cloud. We use a constant value of $T_s = 40$ K across the field. An image of column density in the R-C cloud is shown in Figure 5. The mean column density over the entire structure is $2.0 \pm 1.4 \times 10^{20}$ cm^{-2}. The densest regions are in the body of the cloud at positive latitudes and longitudes. There we measure column densities of $\sim 4 \times 10^{20}$ cm^{-2}, whereas the individual filaments have lower column densities of $\sim 1 \times 10^{20}$ cm^{-2}.

These estimates for the column density and spin temperature allow us to make some order-of-magnitude estimates for

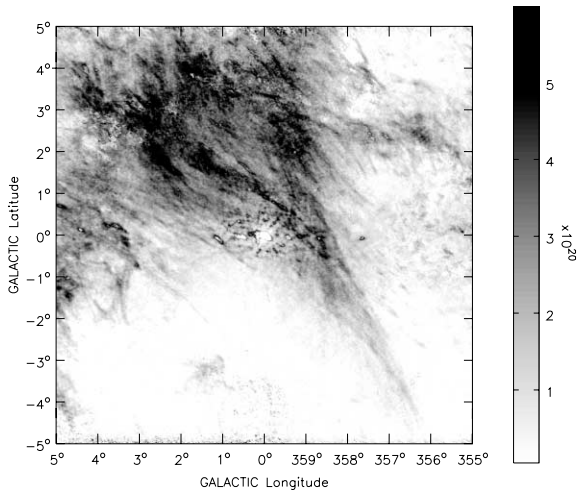

FIG. 5.—H I column density of the R-C cloud assuming a spin temperature of $T_s = 40$ K. The gray scale is displayed in the wedge at the right in units of 10^{20} cm^{-2}.

the density and thermal pressure of the cloud, assuming a cloud thickness, Δs. Crutcher & Lien (1984) based on stellar absorption measurements, estimate that the thickness of the R-C cloud is 1–5 pc. However, our images show that the individual filaments have plane-of-sky widths of less than ~0.1 pc. It is therefore possible that the strands are cylindrical and that the thickness of the strands is similar to the strand width, $\Delta s \sim 0.1$ pc. We therefore use $\Delta s = 0.1$ pc to estimate the H I number density, $n_{\rm H}$, and thermal pressure, $P_{\rm th}/k = N_{\rm H\,I} T_s/\Delta s = n_{\rm H} T_s$ in the individual filaments. The mean H I density and pressure of the filaments are 460 cm^{-3} and 1.8×10^4 K cm^{-3}, respectively. The cylindrical geometry for the strands is more intuitive than a collection of edge-on ribbons. Nevertheless, the data do not exclude an edge-on ribbon scenario. If the filaments are edge-on sheets of width $\Delta s \sim 1$ pc, as suggested from the lower limit of Crutcher & Lien (1984) then the mean H I density and pressure of the filaments are 46 cm^{-3} and 1.8×10^3 K cm^{-3}, respectively. For the upper left of the cloud we suggest that the smoothness is indicative of many filaments integrated along the line of sight. We therefore assume that the width of the base is 1–5 pc, as estimated by Crutcher & Lien (1984). Assuming $\Delta s = 1$–5 pc, the H I density in the base is ~25–130 cm^{-3}, and the pressure is $(1$–$5) \times 10^3$ K cm^{-3}.

The thermal pressure of the filaments in the R-C cloud is almost an order of magnitude larger than that expected for the CNM near the Sun, which is believed to be only $P_{\rm th} \sim 4000$ K cm^{-3} (Wolfire et al. 2003). While it is at first disconcerting to estimate pressures that are so far out of thermal equilibrium, these pressures are not exceptional. Jenkins & Tripp (2001) found that as much as 25% of the neutral carbon-bearing interstellar medium (ISM) has thermal pressures in the range $P/k = 10^{3.5}$–$10^{4.0}$ K cm^{-3} and with a few percent having pressures larger than $P/k = 10^{4.0}$ K cm^{-3}. In most areas of the ISM the thermal pressure is a small fraction of the total pressure. We can estimate the total pressure in the R-C cloud as $P = \sigma^2 \rho$ including both the thermal and turbulent motions, where ρ is the mass density assuming 10% helium, $\rho = 1.4 m_{\rm H} n_{\rm H}$. For $\sigma \approx 1.5$ km s^{-1} and an average number density of $n_{\rm H} \sim 460$ cm^{-4}, the total pressure in the filaments is $P/k \sim 2 \times 10^5$ K cm^{-3}. Again the total pressure is about a factor of 10 larger than total pressure (thermal plus all nonthermal components) for the general ISM in the midplane (Boulares & Cox 1990).

3.1.2. *Density and Pressure Caveats*

It is worth taking note of some of the caveats to the density and pressure estimates given above. These estimates rely on assumptions made about T_s, p, and Δs. Our column density image assumes a constant spin temperature across the cloud. This is almost certainly not true, but in the absence of saturation in the H I profiles it is not possible to solve for T_s and τ for all positions. Letting T_s vary randomly around the image about a mean 40 K with a variance of 10 K we found that the densities measured do not vary significantly from those determined here.

The exact value of $T_s = 40$ K assumed for the spin temperature has an effect on the densities and pressures derived. The cosmic microwave background sets an absolute minimum value for $T_s \geq 2.73$ K, which results in column densities about an order of magnitude smaller than those derived for $T_s = 40$ K. Such a low spin temperature is highly unlikely in almost all Galactic environments where the UV radiation field and cosmic-ray heating raise the temperature well above the CMB background. If we assume that $T_s = 30$ K, which is at the lower end of values estimated by previous authors, then the derived column densities are a factor of ~0.6 smaller than for $T_s = 40$ K. Values of $T_s > 40$ K result in undefined values of τ toward regions where $|\Delta T|$ is large.

The assumed value of p can significantly effect the derived optical depth and column density. By assuming $p = 1$ we have minimized the optical depth for any given value of T_s and therefore minimized the densities and pressures calculated. In addition, values of $p \approx 1$ are most likely given the close proximity of the cloud. If we decrease p to an unlikely value of 0.8 it has two main effects: first, the optical depth becomes undefined over large areas of the map and second, the derived column densities are typically a factor of 2 larger than for $p = 1$.

Finally, the assumed cloud thickness has a large impact on the derived densities and pressures. We have assumed a thickness for the filaments that is an order of magnitude smaller than previous estimates by Crutcher & Lien (1984). However, Crutcher & Lien (1984) used stellar absorption measurements at distances bracketing the cloud to estimate its thickness. Those measurements did not have subparsec precision and they would not have been able to exclude a thickness of less than 1 pc. At the other extreme, if we adopt the Crutcher & Lien (1984) upper limit of $\Delta s = 5$ pc for the filaments, the derived pressures and densities will be a factor of 50 smaller than those derived for $\Delta s \sim 0.1$ pc. This would present a very unusual ribbon-like geometry for the R-C filaments, which we do not believe is likely.

4. THE MAGNETIC FIELD STRUCTURE

The filaments observed here, although curved, have virtually no wiggles. This taughtness suggests that the gas structure may be dominated by some process other than turbulence, such as a magnetic field. To explore this suggestion we have searched for the orientation of the magnetic field associated with the R-C cloud. We used the Heiles (2000) compilation of optical measurements of stellar polarization to determine the magnetic field direction. From Heiles (2000) we extracted all stars at distances of less than 2 kpc in the region $-5^\circ \leq l \leq +5^\circ$, $-5^\circ \leq b \leq +5^\circ$. To ensure reliable polarization angle measurements we further constrained the selection to stars with polarized intensity greater than 1% of the total intensity; 56 stars met the criteria. In Figure 6 we have overlaid polarization vectors on the H I ΔT image of the R-C cloud at $v = 4.95$ km s^{-1}. Vectors are shown at the position of each polarized star, oriented with the polarization

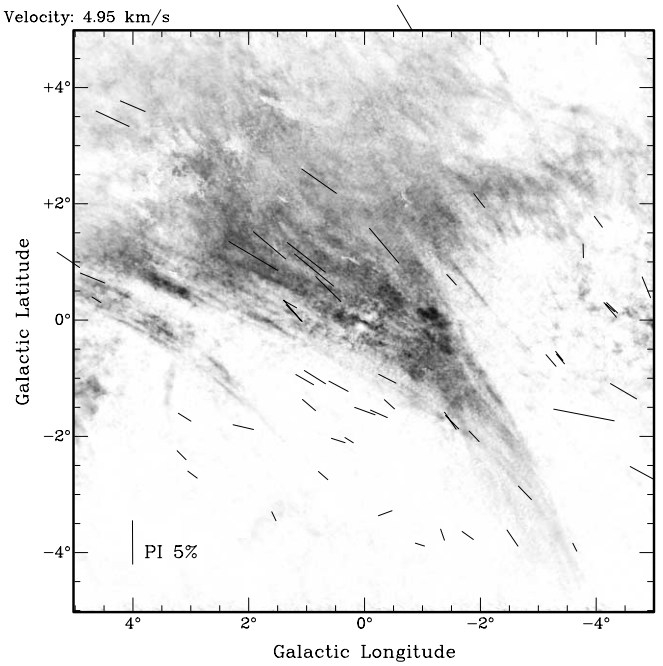

FIG. 6.—H I image of the R-C cloud at $v = 4.95$ km s^{-1} overlaid with vectors of stellar polarization from Heiles (2000). The measured polarization vectors are aligned with the magnetic field direction. The length of the vectors is proportional to the measured fractional polarized intensity, with the scale given by the 5% fractional polarized intensity vector shown by the scale of the vector in the bottom left corner.

angle,[8] θ_p. The length of the vectors is proportional to the measured fractional polarized intensity of the star, with a vector of 5% fractional polarization shown in the key at the bottom left. In the regions covered by the cloud there is a remarkable agreement between the orientation of the polarization vectors and the direction of the cloud's filaments. By contrast, in the area $l \geq -2^\circ$ and $b \leq -3^\circ$ there is very little absorption associated with the cloud and these regions show disordered polarization vectors. Referring only to the area covered by the cloud ($l > -3^\circ$, $b > -3^\circ$), the mean polarization angle is $\langle \theta_p \rangle = 53^\circ \pm 11^\circ$. The polarization angle for polarization arising from polarization of background starlight is parallel to the magnetic field direction such that the angle of the magnetic field, θ_B, also equals $53^\circ \pm 11^\circ$.

Stellar polarization measurements probe the magnetic field integrated along the line of sight, which can lead to a superposition of structures in the observed vectors. Because we initially included all stars out to 2 kpc distance it is also possible that the magnetic field orientation observed is not associated with the R-C cloud, but located behind it. To test this we examined only stars out to a distance of 200 pc and found that, although the sample size is smaller, the mean polarization angle agreed with $\langle \theta_p \rangle = 53^\circ$ to within the standard deviation of the full sample. This suggests that the dominant magnetic structure along this line of sight lies within 200 pc and the very good alignment with the R-C H I strands suggests that they are related.

5. DISCUSSION

5.1. *Magnetic Field Strength*

Measurements of stellar polarization do not directly yield a measurement of the strength of the magnetic field. However, Chandrasekhar & Fermi (1953) suggested that the variance in an ensemble of polarization measurements can be used to estimate the strength of the field. This method is often applied to measurements of starlight polarization due to dust (e.g., Andersson & Potter 2006) and has been tested against theoretical MHD models by Heitsch et al. (2001) and Ostriker et al. (2001). The technique assumes that turbulence in the magnetized medium will randomize the magnetic field and that the stronger the regular field is, the less it is disturbed by turbulence. Using the Chandrasekhar-Fermi (C-F) method, as modified by Heitsch et al. (2001) the strength of the magnetic field in the plane of the sky can be estimated as

$$\langle B \rangle^2 = \xi 4\pi\rho \frac{\sigma_v^2}{\sigma(\tan \delta_p)^2}, \quad (5)$$

where σ_v, is the turbulent line width for the R-C filaments, ρ is the density of the medium, $\delta_p \equiv \theta_p - \langle \theta_p \rangle$, and ξ is a correction factor (e.g., Heitsch et al. 2001). For small values of δ_p, $\sigma(\tan \delta_p) \approx \sigma(\delta_p)$. The derived magnetic field depends on the assumed value for ξ. Heitsch et al. (2001) found that for simulated molecular clouds the value of ξ required to reconcile the C-F estimated field strength and the input field was in the range 0.2–1, with an average value of 0.5 for the ensemble of simulated clouds. Ostriker et al. (2001) also found an average correction factor of 0.5 for simulated molecular clouds, although with a smaller dispersion.

To estimate the magnetic field strength in the R-C cloud we will adopt $\xi = 0.5$. The dispersion in the measured stellar polarization angles toward the R-C cloud is $\sigma(\delta_p) \approx 11^\circ$ and, as before, $\rho = 1.4 m_{\rm H} n_{\rm H} = 1.1 \times 10^{-21}$ g cm^{-3} and $\sigma_v = \sigma_{\rm turb} = 1.4$ km s^{-1}. We therefore estimate that $\langle B \rangle \sim 60$ μG. Because of the uncertainty in the correction factor, ξ, for a given cloud, the field strength estimated from the C-F method must be regarded as a rough estimate, probably only good to within a factor of 2.

As an alternative to the C-F method, we can estimate the magnetic field strength assuming equipartition of the magnetic and kinetic energy densities in the cloud. The R-C cloud filaments appear to be very straight compared with other structures observed in the ISM. Magnetic tension can provide a mechanism for holding filaments straight against turbulent effects. For the magnetic field to dominate the structure it must dominate over internal turbulence and gravitational effects. We can estimate the relative contributions of the kinetic, gravitational, and magnetic energy densities, $\mathcal{KGM}$, respectively. The kinetic energy density for an H I cloud is given by

$$\mathcal{K} = 3/2(1.4 m_{\rm H}) n_{\rm H} \sigma^2 = 2.1 \times 10^{-33} \frac{N_{\rm H} \Delta v^2}{\Delta s} \text{ ergs cm}^{-3}, \quad (6)$$

where Δv is in km s^{-1} and Δs is in pc. Considering just the filaments of the R-C cloud, where $N_{\rm H} \sim 1 \times 10^{20}$ cm^{-2}, $\Delta v \sim 3.5$ km s^{-1}, and $\Delta s \approx 0.07$ pc if the filaments are cylinders, then the kinetic energy density is $\mathcal{K} = 3.7 \times 10^{-11}$ ergs cm^{-3}. If the filaments are edge-on ribbons instead of cylinders then the kinetic energy density will be smaller.

If we approximate the filaments as cylinders of $r = \Delta s/2$ and length L, then the total gravitational energy is given by $W = -GM^2/L$ (Fiege & Pudritz 2000) and the gravitational energy density is

$$\mathcal{G} = G\pi(1.4 m_{\rm H} n_{\rm H} r)^2, \quad (7)$$

[8] The polarization angles are measured such that $\theta_p = 0^\circ$ when the vector points toward up and increases in a clockwise direction.

For the R-C filaments, the gravitational energy density is $\mathcal{G} \sim 3 \times 10^{-15}$ ergs cm^{-3}. The gravitational energy density is very small compared to the kinetic energy density; these filaments are clearly not self-gravitating.

Finally, the magnetic energy density is $\mathcal{M} = |B_{\rm tot}|^2/8\pi$, where $B_{\rm tot} \geq B_{\rm meas}$. Given negligible gravitational energy density, for the magnetic field to dominate the structure observed in the R-C cloud, $\mathcal{M} > \mathcal{K}$. For $\mathcal{K} \sim 3.7 \times 10^{-11}$ ergs cm^{-3} the magnetic field strength must be $B_{\rm tot} > 30$ μG. The agreement between the magnetic field strength derived assuming magnetic dominance and with the C-F method is surprisingly good. One can use this result and equation (5) to solve for ξ for the R-C cloud. A field strength of >30 μG implies that the correction factor, ξ, for this cloud should be >0.12.

To better understand the magnetic field of the R-C cloud we would also require measurements of the line-of-sight magnetic field strength. Most measurements of magnetic fields in the CNM have been made using Zeeman splitting (e.g., Heiles & Troland 2005), which probes the line-of-sight component of the field. Heiles & Troland (2005) find a median CNM magnetic field strength of 6.0 $\pm$ 1.8 μG over a wide range of Galactic environments. This is considerably lower than the values estimated here for the R-C cloud. It is important to note, however, that the density of the R-C cloud is larger than typical CNM values. In fact, the magnetic field strength estimated is more consistent with values obtained for molecular clouds with densities similar to that of the R-C cloud (Crutcher 1999). However, for these measurements it is usually assumed that gravitational contraction compresses the magnetic field lines leading to an increase in density and magnetic field strength. There is no evidence for such action in the R-C cloud and it is therefore curious that it should exhibit such a high magnetic field strength.

5.2. *Comments on the Structure of the CNM*

The structure of the cold neutral medium (CNM) is very difficult to study. For many years we have harbored the notion that the CNM was distributed in isotropic clouds as described in the McKee & Ostriker (1977) paradigm. However, there is a fair amount of evidence against this model. For example, high-resolution H I absorption measurements toward pulsars and radio galaxies find very small-scale variations in the H I that seem to require unreasonably high thermal pressures if we assume they are spherical. Heiles (1997) invoked geometry to explain this "tiny scale atomic structure" (TSAS), suggesting instead that these measurements probe cold gas in thin sheets viewed edge-on or filaments viewed end-on. Although the sheet or filament description is appealing because of its resolution of the over-pressure problem, it has not been readily adopted, owing largely to the lack of observational evidence for counterparts aligned perpendicular to the line of sight. These sheets or filaments are predicted to have very low column densities, rendering them unobservable (Heiles 1997). There is evidence that on larger scales the CNM is indeed in large-scale filaments of sheets. In the few examples where we can image large areas of the CNM through H I self-absorption, such as in the CGPS and SGPS (Gibson et al. 2005; Kavars et al. 2005), the CNM seems extended, with complicated structure that is far from isotropic. H I absorption measurements toward closely separated continuum sources support this view with similar absorption components that suggest extended CNM clouds with aspect ratios $\sim$10–200 (Heiles & Troland 2003). With our images we find that the cold medium of the R-C does not resemble the spherical clouds of McKee & Ostriker (1977) but instead is structurally much closer to the Heiles (1997) description of filaments. Our filaments differ from those proposed by Heiles (1997) in that they are viewed side-on, rather than end-on. Although the size scales represented by the R-C cloud are more than 2 orders of magnitude larger than those observed in TSAS, the R-C cloud presents evidence that the CNM on small scales is structured in filaments with extreme aspect ratios.

5.3. *Comparison with Molecular Clouds*

As much as 60% of the H I self-absorption features observed in the inner Galactic plane have some association with molecular gas as detected by ^{12}CO emission (Kavars et al. 2005). Comparing the H I data with data from the low-resolution (30′) ^{12}CO survey (Dame et al. 1987), there is some indication for associated CO emission at high latitudes around $v \approx 3.5$ km s^{-1}. Without CO data of comparable resolution to the H I it is difficult to make a clear association between the H I self-absorption filaments and CO emission. Although CO emission in the dense base of the R-C cloud seems reasonable, CO emission in the filaments would be surprising. The filaments' column densities of $\sim 1 \times 10^{20}$ cm^{-2} should account for only $\sim$0.05 mag of visual extinction, which is below the extinction limit generally required to shield CO from photodissociation (van Dishoeck & Black 1988).

Despite the lack of clear molecular emission in the filaments, it may be informative to compare the filamentary structure of the R-C cloud with that seen in molecular clouds. Kavars et al. (2005) suggest that gas probed by H I self-absorption may fill the evolutionary gap between diffuse atomic clouds and molecular clouds. The density of the R-C cloud filaments, $n \sim 460$ cm^{-3} is much higher than most H I self-absorption features (Kavars et al. 2005) and indeed most of the CNM (Heiles & Troland 2003); it is instead closer to the low end of molecular cloud densities (Crutcher 1999). Morphologically, the R-C cloud is reminiscent of the structure observed in some molecular clouds. Molecular clouds have long been observed to have elongated filamentary structure similar to that observed in the R-C cloud. Good examples of filamentary molecular clouds are the Taurus, ρ Ophiuchus, and Orion molecular clouds, which show long molecular filaments with dense clumps along their lengths (e.g., Mizuno et al. 1995; Falgarone et al. 2001). Although it is not clear how filamentary structure develops in molecular clouds, it is expected that magnetic fields play an important role in establishing and maintaining their structure.

Far-infrared polarization observations of filamentary molecular clouds show that very often the polarization vectors are oriented either along or perpendicular to the filaments (Matthews & Wilson 2000). This bimodal distribution has often been attributed to helical magnetic fields that wrap around the filaments (Carlqvist & Kristen 1997; Fiege & Pudritz 2000). However, reliably inferring the three-dimensional magnetic field structure from plane-of-sky dust polarization measurements is difficult. Some of the most promising evidence for helical magnetic field structure has come from Zeeman measurements of Orion A (Robishaw & Heiles 2005), which show the field reversing direction on opposite sides of the filament.

A fundamental difference between filamentary molecular clouds and the R-C cold H I filaments is that molecular clouds are in general self-gravitating. Depending on the field geometry the magnetic field in molecular clouds can provide crucial support against gravitational collapse. For example, for fields aligned along the direction of elongation (poloidal fields) the magnetic field provides an outward pressure to counter the gravitational contraction. For helical fields the situation is more complex with the net pressure effect at the surface of the cloud depending on the relative strengths of the poloidal and azimuthal components. For

helical fields where the azimuthal component dominates the magnetic pressure acts inward.

For the R-C cloud the true configuration of the magnetic field is crucial to defining the cloud life-time. It is also particularly difficult to distinguish the field configuration within the cloud from the configuration of the ambient field from the stellar polarization alone. If the field within the filaments is poloidal or helical with a dominant poloidal component, as the observed polarization vectors suggest, then the magnetic field has the effect of increasing the total pressure. The overpressurized filaments should be short-lived with radial crossing times on the order of 4×10^4 yr. If, on the other hand, the field within the filaments is actually helical and has places where the azimuthal field dominates, then the magnetic pressure may stabilize against the thermal pressure and could even lead to collapse and fragmentation of the filaments. Unfortunately it is impossible to infer the true internal magnetic field configuration from the starlight polarization data of these multiple superimposed filaments. Zeeman measurements of the line-of-sight magnetic field component are needed to understand the dynamical future of the R-C cloud.

6. CONCLUSIONS

We have presented new high-resolution H I self-absorption images of part of the Riegel-Crutcher cold cloud at a distance of 125 pc in the direction of the Galactic center. These images, which are part of the SGPS Galactic center survey, cover the area $-5^\circ \leq l \leq 5^\circ$, $-5^\circ \leq b \leq 5^\circ$ with an angular resolution of $100''$. The data reveal extraordinary filamentary structure within the R-C cloud. The cloud seems to be composed of a network of aligned narrow filaments that merge into a smooth mass at the upper left of the cloud. The filaments are very elongated, with the most extreme example only 0.07 pc wide and over 16 pc long. Using saturated absorption profiles in the cloud we estimate a spin temperature for the cloud of $T_s \sim 40$ K, which is similar to values previously estimated by Crutcher & Riegel (1974) and Montgomery et al. (1995). Adopting a spin temperature of 40 K for the entire cloud we created images of the optical depth and column density of the cloud, finding an average column density of $\sim 2 \times 10^{20}$ cm^{-2}. If the individual filaments of the cloud are approximated as cylinders, then their average thermal pressure is $\sim 2 \times 10^4$ K cm^{-3}.

From measurements of the polarization of starlight from Heiles (2000) we have shown that the filaments in the R-C cloud are aligned with the magnetic field of the cloud. Using the Chandrasekhar-Fermi method we have roughly estimated the magnetic field strength to be ~ 60 μG. By comparing ratios of gravitational, kinetic, and magnetic energy densities we show that the filaments are not self-gravitating. We suggest that the excellent alignment between the filaments and the magnetic field, as well as the straightness of the filaments, is evidence that the magnetic field dominates over thermal and turbulent motions within the cloud. For the magnetic energy density to exceed the kinetic energy density the magnetic field must be >30 μG. Given the uncertainties associated with the Chandrasekhar-Fermi method the two field strengths are fully consistent.

Directly imaging the structure of the CNM is always difficult. The R-C cloud, because it is in front of the bright, high column density H I background toward the Galactic center, provides us with a unique opportunity to directly image the CNM. In this case the CNM appears highly filamentary and most closely resembles the high aspect ratio filaments suggested by Heiles (1997) to explain tiny scale atomic structure. There is no reason to believe that the structure of the R-C cloud is unique; it may in fact be typical for the CNM. We point out that there are morphological similarities between the R-C cloud and filamentary molecular clouds, which are also characterized by strong magnetic fields. If gas traced by H I self-absorption is either a precursor to molecular gas or formed from dissociation of molecular clouds the morphological similarity is not surprising.

The Parkes Radio Telescope and the Australia Telescope Compact Array are part of the Australia Telescope which is funded by the Commonwealth of Australia for operation as a National Facility managed by CSIRO. This work was supported by NSF grants AST 03-07358 to Harvard University and AST 03-07603 to the University of Minnesota. M. H. acknowledges support from the National Radio Astronomy Observatory (NRAO), which is operated by Associated Universities Inc., under cooperative agreement with the National Science Foundation. The authors thank an anonymous referee for insightful and interesting questions and suggestions.

REFERENCES

Andersson, B-G, & Potter, S. B. 2006, ApJ, 640, L51
Boulares, A., & Cox, D. P. 1990, ApJ, 365, 544
Carlqvist, P., & Kristen, H. 1997, A&A, 324, 1115
Chandrasekhar, S., & Fermi, E. 1953, ApJ, 118, 116
Crutcher, R. M. 1999, ApJ, 520, 706
Crutcher, R. M., & Lien, D. J. 1984, in IAU Colloq. 81, Local Interstellar Medium, ed. Y. Kondo, F. C. Bruhweiler, & B. D. Savage (Washington: NASA), 117
Crutcher, R. M., & Riegel, W. K. 1974, ApJ, 188, 481
Dame, T. M., Ungerechts, H., Cohen, R. S., de Geus, E. J., Grenier, I. A., May, J., Murphy, D. C., Nyman, L. A., & Thaddeus, P. 1987, ApJ, 322, 706
Falgarone, E., Pety, J., & Phillips, T. G. 2001, ApJ, 555, 178
Fiege, J. D., & Pudritz, R. E. 2000, MNRAS, 311, 85
Gibson, S. J., Taylor, A. R., Higgs, L. A., Brunt, C. M., & Dewdney, P. E. 2005, ApJ, 626, 195
Gibson, S. J., Taylor, A. R., Higgs, L. A., & Dewdney, P. E. 2000, ApJ, 540, 851
Heeschen, D. S. 1955, ApJ, 121, 569
Heiles, C. 1997, ApJ, 481, 193
———. 2000, AJ, 119, 923
Heiles, C., & Troland, T. H. 2003, ApJ, 586, 1067
———. 2005, ApJ, 624, 773
Heitsch, F., Zweibel, E. G., Mac Low, M.-M., Li, P., & Norman, M. L. 2001, ApJ, 561, 800
Jenkins, E. B., & Tripp, T. M. 2001, ApJS, 137, 297
Kavars, D., Dickey, J. M., McClure-Griffiths, N. M., Gaensler, B. M., & Green, A. J. 2003, ApJ, 598, 1048
Kavars, D., Dickey, J. M., McClure-Griffiths, N. M., Gaensler, B. M., & Green, A. J. 2005, ApJ, 626, 887
Levinson, F. H., & Brown, R. L. 1980, ApJ, 242, 416
Lindblad, P. O., Grape, K., Sandqvist, A., & Schober, J. 1973, A&A, 24, 309
Matthews, B. C., & Wilson, C. D. 2000, ApJ, 531, 868
McClure-Griffiths, N. M., Dickey, J. M., Gaensler, B. M., Green, A. J., Haverkorn, M., & Strasser, S. 2005, ApJS, 158, 178
McKee, C. F., & Ostriker, J. P. 1977, ApJ, 218, 148
Mizuno, A., Onishi, T., Yonekura, Y., Nagahama, T., Ogawa, H., & Fukui, Y. 1995, ApJ, 445, L161
Montgomery, A. S., Bates, B., & Davies, R. D. 1995, MNRAS, 273, 449
Ostriker, E. C., Stone, J. M., & Gammie, C. F. 2001, ApJ, 546, 980
Reynolds, J. E. 1994, ATNF Tech. Rep. AT/39.3/0400 (Sydney: ATNF)
Riegel, K. W., & Crutcher, R. M. 1972, A&A, 18, 55
Riegel, K. W., & Jennings, M. C. 1969, ApJ, 157, 563
Robishaw, T., & Heiles, C. 2005, BAAS, 37, 1493
Sault, R. J., & Killeen, N. E. B. 2004, The Miriad User's Guide (Sydney: ATNF)
Sault, R. J., Staveley-Smith, L., & Brouw, W. N. 1996, A&AS, 120, 375
Stanimirović, S. 2002, in ASP Conf. Ser. 278, Single-Dish Radio Astronomy: Techniques and Applications, ed. S. Stanimirović et al. (San Francisco: ASP), 375
Taylor, A. R., et al. 2003, AJ, 125, 3145
van Dishoeck, E. F., & Black, J. H. 1988, ApJ, 334, 771
Wolfire, M. G., McKee, C. F., Hollenbach, D., & Tielens, A. G. G. M. 2003, ApJ, 587, 278